Large Variation of Dirac Semimetal State in Perovskite $CaIrO_3$ with Pressure-Tuning of Electron Correlation

R. Yamada,[1] J. Fujioka,[2] M. Kawamura,[3] S. Sakai,[3] M. Hirayama,[3] R. Arita,[1,3] T. Okawa,[1] D. Hashizume,[3] M. Hoshino,[3] and Y. Tokura[1,3,4]

[1]*Department of Applied Physics, University of Tokyo, Tokyo 113-8656, Japan*
[2]*Faculty of Pure and Applied Sciences, University of Tsukuba, Tsukuba 305-8577, Japan*
[3]*RIKEN Center for Emergent Matter Science (CEMS), Wako 351-0198, Japan*
[4]*Tokyo College, University of Tokyo, Tokyo 113-8656, Japan*

(Received 24 May 2019; revised manuscript received 16 September 2019; published 19 November 2019)

The impact of electron correlation on the Dirac semimetal state is investigated for perovskite $CaIrO_3$ in terms of the magnetotransport properties under varying pressures. The reduction of electron correlation with a pressure of 1 GPa enhances the Fermi velocity as much as 40%, but it reduces the mobility by an order of magnitude by detuning the Dirac node from the Fermi energy. Moreover, the giant magnetoresistance at the quantum limit due to the one-dimensional confinement of Dirac electrons is critically suppressed under pressure. These results indicate that the electron correlation is a crucial knob for controlling the transport of a correlated Dirac semimetal.

DOI: 10.1103/PhysRevLett.123.216601

The relativistic Dirac-Weyl electron in a solid plays a key role in topological quantum materials exemplified by topological insulators and Dirac-Weyl semimetals [1,2]. The low energy excitation of Dirac-Weyl semimetals is characterized by the massless Dirac band dispersion. Remarkable features of a highly mobile Dirac-Weyl electron show up in various transport phenomena, such as magnetoresistance (MR) and the anomalous Hall effect [3–11]. Since the topological band structure is strongly tied to the crystal, inversion, and/or time-reversal symmetry, their transport phenomena can be critically modified by the symmetry change of the crystal structure or by the application of an external field. For example, the Dirac semimetal is turned into a Weyl semimetal under a magnetic field, which manifests itself as the chiral-anomaly-induced magnetoresistivity [3,4], as demonstrated in Cd_3As_2 and Na_3Bi [5–9]. Another promising knob to control the Dirac-Weyl electron is the electron correlation effect. It has been proposed that this effect may lead to a k-nonlinear deformation or dynamical mass gap of the Dirac cone in two-dimensional Dirac semimetals [12–17], or cause a topological change of band structure in three-dimensional Dirac-Weyl semimetals in proximity to the Mott transition [18–23]. Therefore, the quantum transport phenomena of Dirac-Weyl electron can be critically controlled by the electron correlation, but it has rarely been demonstrated experimentally so far.

The Dirac semimetal state of perovskite iridate $AIrO_3$ (A = Ca, Sr, and Ba) offers a rare opportunity to study the quantum transport of Dirac-Weyl electrons in a strongly correlated region near the Mott transition. In $AIrO_3$, Ir^{4+} with the formal electron configuration $5d^5$ constitutes the orthorhombic perovskite structure of space group $Pbnm$, as illustrated in Fig. 1(a), which yields a nearly half-filled $J_{\mathrm{eff}} = 1/2$ band near the Fermi energy (E_F). The $J_{\mathrm{eff}} = 1/2$ state is characterized by both strong electron correlation and relativistic spin-orbit interaction, harboring the Dirac line node as illustrated in Fig. 1(b). It has been theoretically predicted that since the Dirac line node is protected by the nonsymmorphic crystal symmetry of $Pbnm$, it thus would be robust against perturbations that keep the symmetry intact [23–25]. $AIrO_3$ shows a paramagnetic semimetallic behavior [26–28], and the Dirac-like band dispersion is observed for a thin film sample of $SrIrO_3$ [29]. A recent study based on transport measurements combined with a theoretical calculation proposed that the Dirac line node would be closely tuned to E_F and would yield highly mobile electrons exceeding a mobility of 60 000 $cm^2/V\,s$ for $CaIrO_3$ with a stronger electron correlation [30]. The finely tuned Dirac line node enables us to reach the quantum limit (QL) at a modest magnetic field of about 9 T, wherein the field-induced quasi-one-dimensional (1D) confinement of electrons in the lowest Landau level gives rise to a giant positive MR with a MR ratio exceeding 5500% at 2 K and 14 T. Specifically, a theoretical calculation shows that the Fermi velocity v_F of the Dirac dispersion is significantly renormalized by the electron correlation due to the criticality of the Mott transition. In other words, such a Dirac band structure could be manipulated to a large extent by controlling the electron correlation strength, although it has not been observed to date. Here we demonstrate that the Dirac band-dispersion and transport properties in $CaIrO_3$ are extremely sensitive to a change in the electron correlation effect, which can be finely controlled by hydrostatic

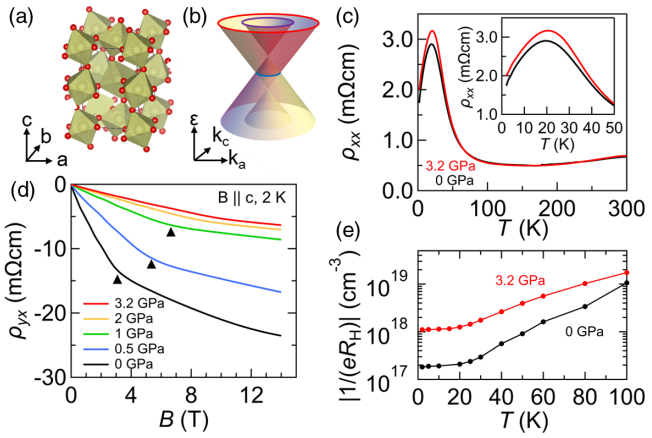

FIG. 1. (a) An illustration of the crystal structure of orthorhombic perovskite $CaIrO_3$. (b) Schematic view of Dirac-like dispersion in the k_a-k_c plane near the line node (blue line). The purple (red) circle denotes the inner FS (outer FS) at the E_F. (c) Temperature dependence of the resistivity under 0 and 3.2 GPa. (Inset) Magnified view of the low temperature region. (d) The Hall resistivity at 2 K under various pressures. (e) Temperature dependence of the inverse Hall coefficient $|1/eR_H|$ as a measure of the carrier density at 0 and 3.2 GPa.

pressure. The magnetotransport measurements and the theoretical calculations suggest that a reduction in electron correlation pulls apart the Dirac line node from the Fermi energy and increases Fermi velocity of the Dirac electron, which results in a large reduction of the Dirac electron mobility as well as a vanishing of the giant positive MR at the QL.

Single crystals of perovskite $CaIrO_3$ were synthesized under high pressure (1 GPa) at 1200 °C using the cubic anvil-type facility [30]. We measured longitudinal resistivity (ρ_{xx}) and Hall resistivity (ρ_{yx}) using the four-terminal method from 2 to 300 K. The sample is installed into a CuBe-type cylinder with Daphne 7373 oil for the measurements under hydrostatic pressure. We note that a small tilting of the sample inside the pressure cell does not affect the results [31]. The electronic structure is calculated with density functional theory (DFT) combined with the dynamical mean-field theory (DMFT) [32], which takes account of the on-site Coulomb interaction. In the DFT calculation, we used the Perdew-Burke-Ernzerhof exchange-correlation functional [33] in the WIEN2K program [31,34].

Application of pressure is a well-established tool for controlling electron correlation. Hydrostatic pressure usually enhances bandwidth (W) via the change of $GdFeO_3$-type lattice distortion in orthorhombic perovskite oxides [37,38], effectively reducing the electron correlation effect measured by U/W. Figure 1(c) shows the temperature (T) dependence of ρ_{xx} at 0 and 3.2 GPa. ρ_{xx} shows a metallic behavior above 150 K, but a prominent peak at around 20 K. The density of thermally activated carriers decreases with lowering T and becomes almost constant below 10 K, whereas mobility increases with lowering T; the counterbalance of these two quantities appears to cause the peak of ρ_{xx} at 20 K [30]. Under pressure, ρ_{xx} does not significantly change above 50 K, while it shows a small enhancement at low T, as shown in the Fig. 1(c) inset. On the contrary, ρ_{yx} changes remarkably with pressure. Figure 1(d) shows ρ_{yx}, which is measured by applying the magnetic field (electric current) along the c axis (a axis) at 2 K. ρ_{yx} is linear with the magnetic field in the low field region but shows a kink at around 3 T. As the pressure increases, the slope of ρ_{yx} decreases and the kink structure gradually becomes blurred. At 3.2 GPa, the kink is no longer clear, and the ρ_{yx}-B curve becomes smooth. We note that the presence of a phase transition or the anomalous Hall effect is not evident, and that the kink corresponds rather to the threshold of the QL of the inner Fermi surface (FS) of the Dirac line node (see also Supplemental Material [31]). Although $CaIrO_3$ is a semimetal with multiple carriers, it has been demonstrated that the charge transport in the lower field region is governed by electrons of the inner FS, which show the lowest density and highest mobility among the carriers [30]. In other words, the carrier density of the inner FS can be approximately estimated using the Hall coefficient R_H in the low field region using the single carrier model (see also the Supplemental Material [31]). Figure 1(e) shows the T dependence of $|1/eR_H|$ as a measure of the carrier density. At 0 GPa, $|1/eR_H|$ decreases with lowering T and is nearly constant below 20 K [30,39]. A similar T dependence is observed at 3.2 GPa, but $|1/eR_H|$ at low T is much larger than that at 0 GPa. We define the carrier density n_e by $|1/eR_H|$ and calculate the electron mobility μ_e. Figure 2(a) shows the pressure dependence of n_e and μ_e at 2 K. At 0 GPa, n_e and μ_e are estimated to be 1×10^{17} cm^{-3} and 4.2×10^4 cm^2/V s, respectively. With increasing pressure, n_e is rapidly enhanced and reaches 8×10^{17} cm^{-3} at 3.2 GPa, whereas μ_e is dramatically reduced down to 4×10^3 cm^2/V s. This contrasts with the pressure effect on the conventional correlated metals, where the application

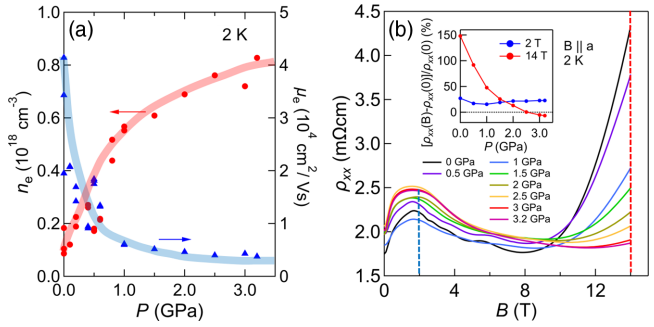

FIG. 2. (a) Pressure dependence of the carrier density n_e (left axis) and mobility μ_e (right axis) at 2 K. (b) The MR under various pressures at 2 K. (Inset) Pressure dependence of the MR ratio $([\rho_{xx}(B) - \rho_{xx}(0)]/\rho_{xx}(0))$ at 2 and 14 T (blue and red dashed lines).

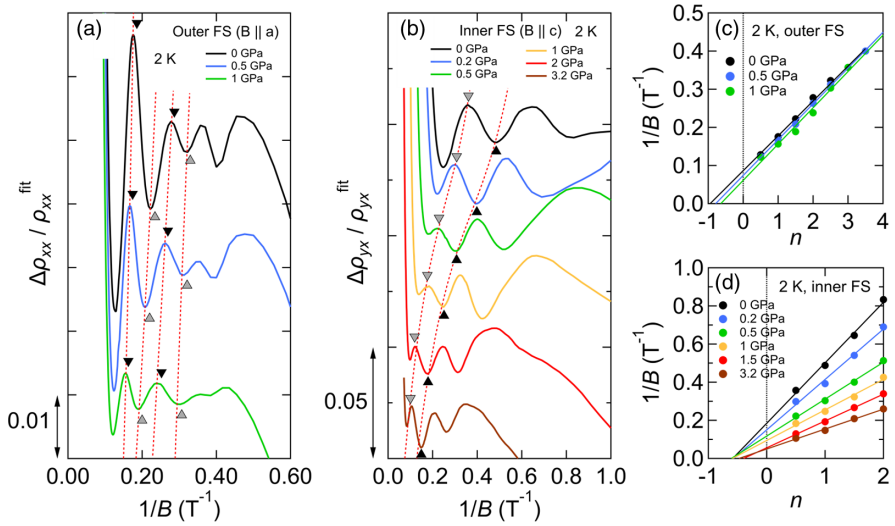

FIG. 3. Oscillatory component of Shubnikov–de Haas oscillations of (a) the outer FS and (b) the inner FS around the Dirac line node under various pressures, with offsets for clarity. Black (gray) triangles denote the positions where the Landau index is an integer (half-integer). Red dotted lines are a guide for the eye. The oscillatory component is derived by dividing by the nonoscillating component after subtraction of the nonoscillating component from the raw data. The Landau index plot of (c) the outer FS and (d) the inner FS under various pressures.

of pressure tends to increase the carrier mobility while keeping the carrier density constant.

The MR also shows a remarkable change under pressure, as shown in Fig. 2(b). Here we applied both the magnetic field and the electric current along the a axis. At 0 GPa, with increasing the magnetic field, ρ_{xx} initially increases up to about 2 T and then moderately decreases, accompanying the Shubnikov–de Haas (SdH) oscillation from the outer FS up to 8 T. Above 8 T, ρ_{xx} abruptly increases, wherein the electrons of the outer FS reach the QL, and hence all of the Dirac electrons start to occupy the lowest Landau level (LL), which is attributed to the field-induced quasi-1D confinement of the Dirac electrons [30]. Interestingly, the large positive MR is rapidly suppressed under pressure and nearly diminishes above 3 GPa. The Fig. 2(b) inset exemplifies the MR ratio $([\rho_{xx}(B)-\rho_{xx}(0\mathrm{T})]/\rho_{xx}(0\mathrm{T}))$ at $B=2$ and 14 T plotted as a function of pressure. At 14 T, the MR ratio exceeds 150% at 0 GPa but decreases to 0% at around 2.5 GPa, further showing a slightly negative (−7%) MR at 3.2 GPa. This is in contrast to the MR at a lower magnetic field prior to the QL, e.g., 2 T, which is nearly independent of pressure.

Figures 3(a) and 3(b) show the SdH oscillations of the outer FS and inner FS, respectively, at various pressures. The oscillation component is derived by subtracting the nonoscillating background from the raw data, which is shown after normalization by the nonoscillating component. Here we note that the SdH oscillation of the inner FS is clearly observed in ρ_{yx} as well as in the MR for $B\|c$ (Figs. S1 and S2 in the Supplemental Material [31]). The oscillation amplitude of the outer FS gradually decreases with increasing the pressure and eventually diminishes above 1.5 GPa. The peak and dip positions of the oscillation slightly shift to a smaller value of $1/B$, i.e., to a higher magnetic field region, and their interval appears to be nearly pressure independent. Similarly, the peak and dip positions of the inner FS moderately shift toward a smaller value of $1/B$ with pressure. The oscillation amplitude of the inner FS is moderately reduced under pressure, but it remains finite even at 3.2 GPa. The MR for $B\|c$ shows a similar oscillation, albeit with a smaller amplitude [Fig. S2(a) in the Supplemental Material [31]]. These results suggest that the inner FS is less subject to the pressure-induced dehancement of scattering time than the outer FS is. In order to quantify the variation of the Fermi surface, we plot the LL fan diagram for the outer and inner FSs in Figs. 3(c) and 3(d), respectively, and determine the oscillation frequency B_F and phase shift ϕ following the Lifshitz-Onsager quantization rule, in which $B_F/B=n-\phi$ with integer n. Here the peak (dip) and dip (peak) positions of $\Delta\rho_{xx}/\rho_{xx}$ ($\Delta\rho_{yx}/\rho_{yx}$) are assigned to integers and half-integers, respectively. The fan plots of both the outer and the inner FS appear to be approximately linear with n, indicating that the effect of Zeeman splitting can be ignored. At 0 GPa, the extracted B_F for the outer FS (inner FS) is 10.9 T (3.5 T), which corresponds to the extreme cross-section area of Fermi surface $S_F=1.0\times10^{-3}$ Å^{-2} (3.3×10^{-4} Å^{-2}). The slope of the fan plot for the outer FS is nearly independent of pressure, while that of the inner FS monotonically decreases with increasing the pressure. ϕ appears to increase slightly under pressure for both the outer and inner FSs. As shown in Fig. 4(a), the S_F of the inner FS increases monotonically with applied pressure

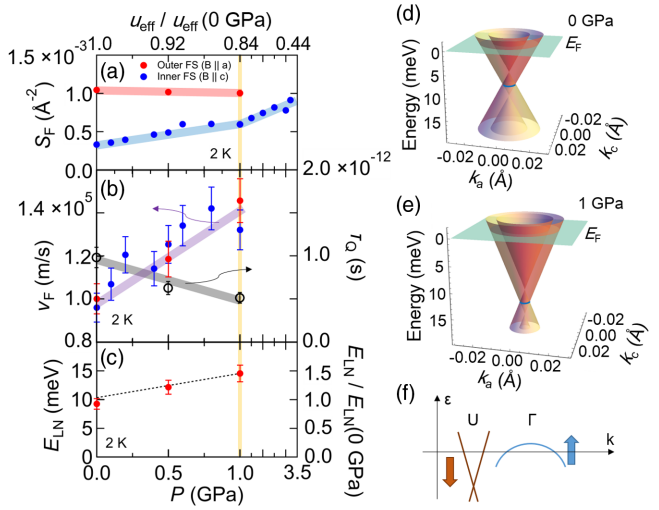

FIG. 4. (a) Pressure dependence of the cross section area S_F of the Fermi surface. (b) The Fermi velocity v_F, and (c) the energy of the line node E_{LN} measured from the Fermi energy. Red (blue) circles are the experimental results of the outer (inner) FS. The dashed line represents an extrapolated line calculated using the DFT + DMFT. The open circles in (b) represent the scattering time τ_Q of the outer FS estimated from the SdH oscillation analysis. The colored broad lines in (a) and (b) are a guide for the eye. The band structures near the Dirac line nodes (d) at ambient pressure and (e) at 1 GPa. Light green planes denote the Fermi level. (f) Sketch of the band structure around the U and Γ points. As pressure is applied, the band around the U point shifts downward, while that around the Γ point shifts upward as a result of carrier compensation's obeying the Luttinger sum rule.

and triples at 3.2 GPa. This contrasts with the case of the outer FS, which remains nearly the same under pressure.

From the thermal damping of amplitude [Figs. S3(a) and S3(b) in the Supplemental Material [31]] [40,41], we derived the cyclotron mass m_c to be 0.21 m_0 (0.13 m_0), with m_0 being the bare electron mass and the Fermi velocity $v_F = 1.0 \times 10^5$ m/s (1.0×10^5 m/s) for the outer FS (inner FS) at 0 GPa. We note that v_F is nearly identical, as expected, between the two FSs within experimental accuracy. With increasing pressure, the m_c of the outer FS (inner FS) is reduced to 0.14 m_0 (0.12 m_0) at 1 GPa. Consequently, the v_F of both FSs increases nearly in parallel with pressure and reaches about 1.4×10^5 m/s at 1 GPa, which is larger by 40% than that at 0 GPa [Fig. 4(b)]. Given that both the inner and outer bands remain k linear under pressure, the energy of the line node (E_{LN}) measured from the Fermi energy increases from 9 meV (0 GPa) to 15 meV (1 GPa) [Fig. 4(c)]. Figures 4(d) and 4(e) illustrate the essence of the pressure variation of the band structure around the Dirac line node.

The theoretical calculation on the basis of DFT + DMFT demonstrates that the v_F is scaled by the renormalization factor due to the electron correlation and thus can be a good measure of electron correlation [30,31]. At 0 GPa, from the comparison between the experiment and the DFT + DMFT results, the effective on-site Coulomb interaction U_{eff} is estimated to be about 1.8 eV. Here we define the effective electron correlation $u_{eff} = U_{eff}/W$ normalized by the bandwidth W. To clarify the correspondence between the pressure and u_{eff}, we plotted the calculated v_F as a function of u_{eff}/u_{eff} (0 GPa) so as to fit the experimental result [Fig. 4(b)]. The pressure reduces u_{eff}/u_{eff} (0 GPa) to 0.84 at 1 GPa. This is in accord with the pressure-induced enhancement of W due to the anticipated reduction of $GdFeO_3$-type distortion [37,38]. We also compare the E_{LN} of experiment and theory. As described above, the E_{LN} increases, by 60% at 1 GPa. This increasing rate is consistent with the theoretical result (50%) when we normalize the E_{LN} by its value at 0 GPa [Fig. 4(c)], though the overall scale of the E_{LN} itself appears larger in theory.

Finally, we discuss the pressure-induced reduction of the giant MR at the QL. As argued previously [30], the giant MR originates from the magnetically induced quasi-1D confinement at the QL of the outer FS. The threshold of the QL is determined by the cross section S_F of the outer FS. Therefore, one might consider the possibility that the onset of giant MR would shift toward a higher magnetic field than the upper limit of our measurement (14 T) if the S_F were enhanced under pressure. This, however, is not the case since the S_F of the outer FS shows little pressure variation, as shown in Fig. 4(a). The observed anomalous reduction of the giant MR is related to the fact that the mobility decreases rapidly under pressure. As described above, the enhancement of the v_F under pressure reduces the m_c for both the outer and inner FSs. Since the mobility is described by the relaxation time divided by the transport mass within semiclassical theory, this means that the relaxation time is reduced by the application of pressure. Indeed, the quantum relaxation time τ_Q of the outer FS, which is derived from an analysis of the Dingle plot of the quantum oscillation, rapidly decreases under pressure, as shown in Fig. 4(b). Because of the Luttinger sum rule, the enhancement of the total electron density of the Dirac bands (a summation of the outer and inner FSs) under pressure suggests that the electrons are transferred from other bands. Indeed, the DFT + DMFT results show that, with a decreasing U_{eff}, the flat valence band around the Γ point shifts toward higher energy and enlarges the hole-pocket FS as illustrated in Fig. 4(f) [30]. The emergence of such a band with a relatively large density of states would significantly promote the intervalley electron scattering between the U and Γ points, leading to a reduction of τ_Q with pressure. In other words, it is likely that the enhanced intervalley electron scattering, triggered by a reduction of the effective electron correlation, reduces the electron mobility and smears out the Landau levels of the outer FS, which results in the disappearance of the giant MR in the QL as well.

In summary, we have demonstrated that the mobility of Dirac electrons can be controlled by an order of magnitude

by the modest hydrostatic pressure in the correlated Dirac semimetal of perovskite $CaIrO_3$. Magnetotransport measurements combined with a theoretical calculation have revealed that a modest pressure of 1 GPa effectively reduces the electron correlation and enhances the Fermi velocity of Dirac dispersion by as much as 40%. An analysis of the quantum oscillation has suggested that the reduction of electron correlation detunes the energy of the Dirac line node from the Fermi level and promotes the intervalley electron scattering, leading to a vanishing of the giant positive MR at the QL. These results suggest that electron correlation is a key parameter for controlling the emergent quantum transport in Dirac semimetals of a strongly correlated region near the Mott criticality.

The authors thank A. Tsukazaki, M. Kawasaki, N. Nagaosa, M. Tokunaga, S. Ishiwata, A. Yamamoto, M. Masuko, and R. Kaneko for the fruitful discussions. This work was supported by the Japan Society for the Promotion of Science (KAKENHI; Grants No. 16H00981, No. 18H04214, and No. 18H01171) from the MEXT, and by PRESTO (Grant No. JPMJPR15R5) and CREST (Grant No. JPMJCR16F1), Japan Science and Technology Agency.

[1] M. Z. Hasan and C. L. Kane, Rev. Mod. Phys. **82**, 3045 (2010).
[2] N. P. Armitage, E. J. Mele, and A. Vishwanath, Rev. Mod. Phys. **90**, 015001 (2018).
[3] H. B. Nielsen and M. Ninomiya, Phys. Lett. **130B**, 389 (1983).
[4] D. T. Son and B. Z. Spivak, Phys. Rev. B **88**, 104412 (2013).
[5] J. Xiong, S. K. Kushwaha, T. Liang, J. W. Krizan, M. Hirschberger, W. Wang, R. J. Cava, and N. P. Ong, Science **350**, 413 (2015).
[6] C. Z. Li, L. X. Wang, H. Liu, J. Wang, Z. M. Liao, and D. P. Yu, Nat. Commun. **6**, 10137 (2015).
[7] H. Li, H. He, H. Z. Lu, H. Zhang, H. Liu, R. Ma, Z. Fan, S. Q. Shen, and J. Wang, Nat. Commun. **7**, 10301 (2016).
[8] C. Zhang, E. Zhang, W. Wang, Y. Liu, Z. G. Chen, S. Lu, S. Liang, J. Cao, X. Yuan, L. Tang, Q. Li, C. Zhou, T. Gu, Y. Wu, J. Zou, and F. Xiu, Nat. Commun. **8**, 13741 (2017).
[9] S. Nishihaya, M. Uchida, Y. Nakazawa, K. Akiba, M. Kriener, Y. Kozuka, A. Miyake, Y. Taguchi, M. Tokunaga, and M. Kawasaki, Phys. Rev. B **97**, 245103 (2018).
[10] T. Suzuki, R. Chinsnell, A. Devarakonda, Y. T. Liu, W. Feng, D. Xiao, J. W. Lynn, and J. G. Checkelsky, Nat. Phys. **12**, 1119 (2016).
[11] E. Liu *et al.*, Nat. Phys. **14**, 1125 (2018).
[12] D. C. Elias, R. V. Gorbachev, A. S. Mayorov, S. V. Morozov, A. A. Zhukov, P. Blake, L. A. Ponomarenko, I. V. Grigorieva, K. S. Novoselov, F. Guinea, and A. K. Geim, Nat. Phys. **7**, 701 (2011).
[13] Z. Q. Li, E. A. Henriksen, Z. Jiang, Z. Hao, M. C. Martin, P. Kim, H. L. Stormer, and D. N. Basov, Nat. Phys. **4**, 532 (2008).
[14] A. Luican, G. Li, and E. Y. Andrei, Phys. Rev. B **83**, 041405(R) (2011).
[15] J. Gonzalez, F. Guinea, and M. A. H. Vozmediano, Phys. Rev. B **59**, R2474 (1999).
[16] M. Hirata, K. Ishikawa, K. Miyagawa, M. Tamura, C. Berthier, D. Basko, A. Kobayashi, G. Matsuno, and K. Kanoda, Nat. Commun. **7**, 12666 (2016).
[17] D. V. Khveshchenko, Phys. Rev. Lett. **87**, 246802 (2001).
[18] X. Wan, A. M. Turner, A. Vishwanath, and S. Y. Savrasov, Phys. Rev. B **83**, 205101 (2011).
[19] W. Witczak-Krempa, A. Go, and Y. B. Kim, Phys. Rev. B **87**, 155101 (2013).
[20] E. G. Moon, C. Xu, Y. B. Kim, and L. Balents, Phys. Rev. Lett. **111**, 206401 (2013).
[21] R. Schaffer, E. K. H. Lee, B. J. Yang, and Y. B. Kim, Rep. Prog. Phys. **79**, 094504 (2016).
[22] K. Ueda, R. Kaneko, H. Ishizuka, J. Fujioka, N. Nagaosa, and Y. Tokura, Nat. Commun. **9**, 3032 (2018).
[23] M. A. Zeb and H.-Y. Kee, Phys. Rev. B **86**, 085149 (2012).
[24] Y. Chen, H. S. Kim, and H. Y. Kee, Phys. Rev. B **93**, 155140 (2016).
[25] C. Fang, Y. Chen, H. Y. Kee, and L. Fu, Phys. Rev. B **92**, 081201(R) (2015).
[26] J. M. Longo, J. A. Kafalas, and R. J. Arnott, J. Solid State Chem. **3**, 174 (1971).
[27] K. Ohgushi, T. Yagi, H. Gotou, Y. Kikuchi, and Y. Ueda, Physica (Amsterdam) **404B**, 3261 (2009).
[28] J. G. Cheng, J. S. Zhou, J. B. Goodenough, Y. Sui, Y. Ren, and M. R. Suchomel, Phys. Rev. B **83**, 064401 (2011).
[29] Y. F. Nie, P. D. C. King, C. H. Kim, M. Uchida, H. I. Wei, B. D. Faeth, J. P. Ruf, J. P. C. Ruff, L. Xie, X. Pan, C. J. Fennie, D. G. Schlom, and K. M. Shen, Phys. Rev. Lett. **114**, 016401 (2015).
[30] J. Fujioka, R. Yamada, M. Kawamura, S. Sakai, M. Hirayama, R. Arita, T. Okawa, D. Hashizume, M. Hoshino, and Y. Tokura, Nat. Commun. **10**, 362 (2019).
[31] See Supplemental Material at http://link.aps.org/supplemental/10.1103/PhysRevLett.123.216601, which includes Refs. [30,32–36], for additional information on the transport measurements, an analysis of quantum oscillation, and the electronic structure calculation.
[32] A. Georges, G. Kotliar, W. Krauth, and M. J. Rozenberg, Rev. Mod. Phys. **68**, 13 (1996).
[33] J. P. Perdew, K. Burke, and M. Ernzerhof, Phys. Rev. Lett. **77**, 3865 (1996).
[34] P. Blaha, K. Schwarz, P. Sorantin, and S. B. Trickey, Comput. Phys. Commun. **59**, 399 (1990).
[35] J. Kuneš, P. Wissgott, and E. Assmann, Comput. Phys. Commun. **181**, 1888 (2010).
[36] A. A. Mostofi, J. R. Yates, Y. S. Lee, I. Souza, D. Vanderbilt, and N. Marzari, Comput. Phys. Commun. **178**, 685 (2008).
[37] M. Imada, A. Fujimori, and Y. Tokura, Rev. Mod. Phys. **70**, 1039 (1998).
[38] Y. Okada, T. Arima, Y. Tokura, C. Murayama, and N. Mori, Phys. Rev. B **48**, 9677 (1993).
[39] J. Fujioka, T. Okawa, A. Yamamoto, and Y. Tokura, Phys. Rev. B **95**, 121102(R) (2017).
[40] D. Shoenberg, *Magnetic Oscillations in Metals* (Cambridge University Press, Cambridge, England, 1984).
[41] G. Landwehr and E. I. Rashba, in *Landau Level Spectroscopy: Modern Problems in Condensed Matter Sciences*, Vol. 27.2 (North-Holland, Amsterdam, 1991).